Impact of flow velocity on denitrification - A plastic tube laboratory experiment

Alexandre Boisson[1,2], Delphine Roubinet[1,3], Luc Aquilina[1], Olivier Bour[1], and Philippe Davy[1]

[1] Géosciences Rennes, UMR CNRS 6118, Université de Rennes 1, Rennes, France

[2] Now at BRGM, D3E/NRE, Indo-French Centre for Groundwater Research, 500 007 Hyderabad India

[3] Now at Applied and Environmental Geophysics Group, University of Lausanne, Lausanne, 1015 Switzerland

Corresponding author: a.boisson@brgm.fr

Abstract

Understanding and predicting hydraulic and chemical properties of natural environments are current crucial challenges. It requires considering hydraulic, chemical, and biological processes and evaluating how hydrodynamic properties impact on biochemical reactions. In this context, we have developed an original plastic-tube laboratory experiment to study the impact of flow velocity on denitrification along a one-dimensional flow streamline. Based on the example of nitrate reduction, nitrate-rich water passes through plastic tubes at several flow velocities (from 6.2 to 35 mm/min), while nitrate concentration at the tube outlet is monitored for more than 500 hours. This experimental setup allows assessing the biologically controlled reaction between a mobile electron acceptor (nitrate) and an electron donor (carbon) coming from an immobile phase (tube) that releases organic carbon during its degradation by

microorganisms. It results in observing various dynamics of nitrate transformation associated with biofilm development where flow velocity appears to be a key factor, as (i) the experiments conducted with the largest flow velocities are characterized by a fast increase of the reactivity rate until reaching a threshold where strong oscillations are observed; and (ii) experiments conducted with a small flow velocity lead to a slow increase of the reactivity rate until reaching a stable threshold value. These main behaviors are related to phases of biofilm development through a simple analytical model based on the assumption that nutrients are incorporated to cells (assimilation). The presented results and their interpretation demonstrate the impact of flow velocity on reaction performance and stability, and highlight the relevance of flow-through experiments over static experiments for understanding biogeochemical processes. The previous aspect is critical as flow velocity may be a key-controlling parameter in systems where mobile water interacts with a growing non-mobile biological phase. This is particularly the case in aquifers where a broad range of flow velocity in pores and fractures is expected in which biochemical reactions, such as autotrophic denitrification with pyrite, can occur.

Keywords: Denitrification; Groundwater; Biofilm; Plastic tube experiment; Channel flow; Analytical model

I. Introduction

Worldwide leaking of agricultural-derived nitrate to groundwater represents a long-term risk for groundwater quality [Khan and Spalding, 2004; Spalding and Exner, 1993]. In this context, natural attenuation of this compound by denitrification has been extensively studied from the batch scale [Kornaros and Lyberatos, 1997; Marazioti et al., 2003] to the aquifer

scale [Clément et al., 2003; Korom, 1992; Tarits et al., 2006]. However, a full understanding of denitrification processes in natural systems requires a structural description of the interactions between hydraulic, chemical, and biological processes at several spatial and temporal scales [Sturman et al., 1995]. Whereas the understanding of reaction kinetics is well developed for static experiments [Hiscock et al., 1991; Korom, 1992], it needs further development for flow-through experiments in order to establish how hydraulic heterogeneities impact reactivity in complex natural media [Tompkins et al., 2001]. Characklis [1981] offers a global discussion on the influence of hydraulic conditions on biofilm development (shape, size and reactive layer) and nutrient availability, and specific experiments have been developed on reactive columns [Sinke et al., 1998; von Gunten and Zobrist, 1993] or simple geometries such as pore networks [Thullner et al., 2002] and tubes [De Beer et al., 1996; Garny et al., 2009; Lewandowski et al., 2007]. These studies focus on relating biofilm development to reactivity processes [De Beer et al., 1996; Garny et al., 2009; Lewandowski et al., 2007] or hydraulic parameters [Beyenal and Lewandowski, 2000; Garny et al., 2009; Lau and Liu, 1993; Stoodley et al., 1994], where the latter experiments are conducted on conduit reactors at the centimeter scale (length and diameter/thickness) with flow velocities with orders of magnitude of 10^2-10^3 mm/min. However, there is a lack of knowledge about the direct impact of fluid velocity on bulk reactivity associated with biochemical reactions in conditions close to natural environments. The previous aspect is critical as flow velocity may be a key-controlling parameter in systems where mobile water interacts with a growing non-mobile biological phase (e.g., autotrophic denitrification with pyrite). This is particularly the case in aquifers where a broad range of flow velocity in pores and fractures is expected.

The global comprehension of hydrodynamic parameters' effects on bioreactivity requires an accurate understanding of their interactions at the laboratory scale. For this

purpose, we propose an experiment in plastic tubes that are equivalent to 1D flow systems where the geometry is perfectly known and the hydraulic parameters are well controlled. Since this experiment is not conducted on natural aquifer material, results and interpretations cannot be directly translated to field applications. For example, it has been established that microorganisms attach more rapidly to hydrophobic and nonpolar surfaces, such as Teflon and other plastics, than hydrophilic materials, such as glass or sand [Donlan, 2002]. It implies that the duration of the attachment period might be shorter in the proposed experiment than in natural environments where the simple geometry of the system might impact attachment as well. As attachment is known to be very difficult to characterize [Cunningham et al., 1991] and remains an unknown to be estimated for each specific case [Donlan, 2002], we do not aim to obtain conclusions concerning this process that occurs in a very short period in comparison to the biofilm-growth period [Singh et al., 2006]. Our study focuses on the biofilm-growth period of long-term experiments and aims at characterizing the impact of hydraulic properties on (i) the efficiency of denitrification along the biofilm-growth period, and (ii) the stability of this biological reaction for bioremediation applications. For this matter, the proposed experiment is the most convenient configuration to assess the influence of hydrodynamic parameters, such as advection along a single flow line, as (i) it simplifies the flow complexity of the system in comparison to column experiments that are a sum of processes occurring on a large number of flow lines; and (ii) it avoids dealing with approximate equivalent parameters as it is usually done for interpreting standard column experiments.

In the proposed experiment, the reactivity evolution of nitrate-rich water passing through PVC tubes is measured for different flow velocities as described in section 2. The hydrodynamic dependence of the experiment results is studied in section 3 and the relationship between biofilm development and reaction processes is analyzed with a simple

93 analytical model in section 4. The impact of flow velocity on biofilm properties and reaction
94 efficiency is then discussed in section 5.

95 # II. Experimental set-up

96 ## 1. Experimental concept

97 Considering denitrification in a system where nitrate flows with water and where the electron
98 donor (such as organic matter or mineral) comes from the soil or rock matrix, we aim to
99 reproduce experimental conditions where the electron acceptor is mobile with water and the
100 electron donor comes from an immobile part. For this purpose, we propose an original
101 biochemical experiment where nitrate-rich water is in contact with plastic tubes that can serve
102 as substrate for heterotrophic bacterial growth [Mohee et al., 2008; Shah et al., 2008]. In the
103 presented experiment, bacteria grow using carbon from the tubes and nitrate from the water,
104 and the denitrification process is reproduced with well-controlled experimental conditions.
105 Although this experiment does not reproduce a natural reaction as done in standard column
106 experiments, it is representative of biochemical reactions characterized by a mobile electron
107 acceptor and an immobile electron donor that have been observed in macropore soils or
108 fractured aquifers (e.g., autotrophic denitrification with pyrite).

109 The simple geometry of the system enables us to know critical parameters such as the
110 real flow velocity and the flow/carbon-source contact area, whereas standard column
111 experiments are related to approximate equivalent parameters. As our experiment is
112 conducted with slow flow velocities (from 6.2 to 35 mm/min) in small diameter tubes (2 mm)
113 in comparison to existing open channel experiments [Garny et al., 2009; Lewandowski et al.,
114 2007], it offers a closer reproduction of pore-scale (or fracture-scale) phenomena. The

115 presented plastic tube experiment is thus an original and convenient experimental set-up
116 characterized by the control of key experimental parameters that are usually not well defined.

117 The water used in the static and flow-through experiments presented in the following
118 section has been collected at the Ploemeur site (Brittany, France). Since 1991, this site
119 provides water to the city of Ploemeur at a rate of 106 m^3 per year [Jiménez-Martínez et al.,
120 2013; Leray et al., 2012] thanks to a contact zone between granite and schist [Ruelleu et al.,
121 2010]. As this water extraction started, an increase of nitrate reduction and sulfate release
122 has been observed in areas where the pumping conditions modified the flow dynamics,
123 whereas concentrations of nitrate remain high in other areas of the system. From the
124 previous observations, Tarits et al. [2006] concluded that natural denitrification due to a
125 heterotrophic denitrification reaction with pyrite was enhanced by forced hydraulic
126 conditions in this site. In order to reproduce this phenomena at the laboratory scale, the
127 presented experiments are conducted with flow velocities in the range of those estimated in
128 the Ploemeur site under pumping conditions [Tarits et al., 2006]. Flow velocities with the
129 same order of magnitude are considered as well for remediation applications [Li et al., 2010]
130 and reactivity assessment [Boisson et al., 2013] in natural environments where reactivity and
131 biofilm development usually occur where the highest velocities are observed.

132 In the presented experiments, the medium inoculation occurs by bacterial attachment
133 and we assume a complete biofilm behavior without considering the diversity of microbial
134 populations and their interaction. Part of the microbial population could come from the tubes
135 since no sterilization was done. Nevertheless, bacteria are supposed to mainly come from the
136 water since (i) they are naturally present in such groundwater [Bekins, 2000; Bougon et al.,

137 2009], and (ii) several experiments with crushed granite and water from the Ploemeur site
138 have shown denitrification processes [Ayraud et al., 2006; Tarits et al., 2006].

139 2. Static experiments

140 Preliminary static (or batch) experiments enable us to identify “reactive” plastic tubes that are
141 able to release carbon to sustain heterotrophic development reactions. 150 ml of the water
142 collected in the Ploemeur site (Brittany, France) is deoxygenated and placed in glass flasks
143 under an argon atmosphere with (i) no plastic tubes, (ii) Pharmed® and Teflon tubes, and (iii)
144 Watson Marlow® PVC double manifold tubes (named PVC tubes). Plastic tube fragments
145 correspond to a mass of 8 g and a reactive surface of 0.018 m^2 and the experiments are
146 conducted in duplicate, which lead to similar results. Nitrate concentration evolves only for
147 the PVC tube experiments where nitrates are completely consumed within 150 hours with a
148 production of organic carbon up to a concentration of 22.03 mg/L after 165 hours (Figure 1).
149 Inorganic carbon shows small variations with a small increase at the beginning of the
150 experiment whereas longer monitoring shows a release of organic carbon up to a
151 concentration of 76.8 mg/L after 378 hours. PVC tubes are thus the carbon source of the
152 observed denitrification reaction that does not occur without the presence of these tubes.

153 3. Experimental conditions for flow-through experiments

154 After demonstrating the PVC tube reactivity with static experiments, flow-through
155 experiments were conducted. The latter experiments consist of (i) continuously injecting
156 nitrate-rich water in PVC tubes, and (ii) monitoring nitrate consumption due to bacterial
157 development through nitrate and nitrite concentration measurements at the tube outlets. The
158 reactive plastic tubes used for the experiments have an inner diameter of 2 mm and a length of

135 cm, and new tubes were used for each experiment. These experiments were performed in the dark at a constant temperature of 18°C and oxygen measurements were done daily.

The nitrate-rich water (45 mg/L) collected in the Ploemeur site (Brittany, France) was not treated before the experiments. Although the water coming from the same piezometer has been sampled at different dates within a year, no water chemistry changes have been observed during this period. This water is almost free of organic carbon with a concentration lower than 0.5 mg/L and the organic carbon concentration in the injected water remains below 0.5 ppm during the whole experiment.

Prior to experimental use, the water is deoxygenated by Argon bubbling and then maintained in anoxic conditions under an argon atmosphere in a high-density polyethylene tank (whose non reactivity is controlled). The entire system is considered as anoxic since no oxygen enters the system either at the inlet or through the tube walls that have a low gas permeability (as indicated by the manufacturer of PVC tubes at page 46 of the documentation available at http://www.watson-marlow.com/Documents/knowledge-hub/Brochures/gb%20-%20UK/Product/Watson%20Marlow%20UK/b-OEM-gb-02.pdf). In addition, the anoxic condition has been verified by measurements of oxygen concentration in water at the tube outlet. As these concentrations remain below the measurable threshold for the whole experiment, we consider that no aerobic degradation occurs in the system.

The water delivered from the tank to the reacting PVC tubes passes through non-reactive Teflon and Pharmed tubes placed in a peristaltic pump (Watson Marlow 205U; Figure 2), where the non-reactivity of the setup before the PVC tubes is checked during all the experiments. The experiments are performed at four different flow rates corresponding to the flow velocities v_1, v_2, v_3 and v_4 equal to 6.2 mm/min, 11, 17 and 35 mm/min, respectively, and are conducted in triplicate for each flow velocity. Such velocities imply residence times in

183 the tubes ranging from 40 minutes to 3 hours and 40 minutes, whereas the whole experiment
184 lasts more than 500 hours.

185 4. Analysis and methods

186 The experiments are monitored by a daily sampling of water inside the tank for the static
187 experiments and at the outlet of the tubes for the flow-through experiments. All samples are
188 filtered with a 0.45 µm Sartorius filter before analyses and major anions (NO_3^-, NO_2^-, SO_4^{2-},
189 Cl^-, and F^-) are analyzed using a Dionex DX 120 ion chromatograph. Organic and inorganic
190 carbons are analyzed every three days using a Shimadzu 5050A Total Organic Carbon
191 analyzer. For all the experiments, the volume used for analyses is equal to 5 ml. In addition,
192 dissolved oxygen is measured using a WTW315i-CondOX probe and daily flow
193 measurements by weighing at the tube outlet show variations below 2% in weighed mass.

194 The limited amount of sampled water prevented us from quantifying gas production in
195 the reactive process (NO, N_2O, and N_2) and biomass concentration flowing out of the tubes.
196 With this simple experimental set up, we assume that (i) the presence of bubbles due to gas
197 formation has a negligible impact on biofilm development and hydraulic properties; and (ii)
198 our interpretation and model can be based only on nitrate and nitrite concentration variation.
199 As explained in section 4, biomass flowing out of the tubes can be taken into account (if
200 needed) in our analytical model with a parameter fitted in regards to the collected
201 measurements. Concerning the assumptions related to bubble formation, the impact of the
202 presence of bubbles has been verified by measuring the velocity of bubbles that are big
203 enough to be observable by the human eye. These velocities are the same as the theoretical
204 mean flow velocity based on water weight measurements and the flow velocity measured at
205 the outlet of the tubes is constant. We thus consider that these bubbles are not trapped into the

biofilm and have a negligible impact on biofilm and hydraulic properties. For the same reasons, we assume as well that potential micro-bubbles (not observable by the human eye) have a negligible impact on these properties. This assumption is coherent with existing studies that show that an impact of bubbles on biofilm and hydraulic properties is less likely in media characterized by large pores [Istok et al., 2007].

III. Experimental results

The nitrate consumption $\Delta C_{NO_3^-}$ (g/L) per unit of volume at time *t* is defined as

$$\Delta C_{NO_3^-}(t) = C_{NO_3^-}^{IN} - C_{NO_3^-}^{OUT}(t), \quad (1)$$

where $C_{NO_3^-}^{IN}$ (g/L) is the initial concentration in the flasks for the static experiments and the concentration measured at the tube inlet for the flow-through experiments, and $C_{NO_3^-}^{OUT}(t)$ (g/L) is the concentration measured at time *t* in the flasks for the static experiments and at the tube outlets for the flow-through experiments. For the latter experiments, no evolution of the nitrate concentration in the tube inlet water has been observed from daily measurements. Therefore, nitrate concentration at the tube inlet ($C_{NO_3^-}^{IN}$) remains constant during the whole experiment (45 mg/L).

Figure 3 represents the nitrate consumption $\Delta C_{NO_3^-}(t)$ (equation 1) for the flow-through experiments where the results obtained with the flow velocities v_1, v_2, v_3 and v_4 are represented by full blue, dashed green, dashdot magenta and dotted red curves, respectively. The presented values correspond to the values averaged over three replicates where all replicates show the same tendency and where error bars represent the mean square deviation.

For static experiments (Figure 1), nitrate concentration in the flask shows a simple behavior as it monotonically decreases until complete consumption within 150 hours. On the contrary, nitrate consumptions observed for flow-through experiments show a more complex behavior (Figure 3a) and seem to be limited by different processes during the experiment. In order to understand which processes impact on nitrate consumption for these experiments, we consider that the evolution of nitrate variation can be roughly decomposed into two phases (Figure 3b). The identified phases are defined and described in detail below, and their relationship to the development of biofilm observed during the experiments (Figure 4) is studied in section 4.

1. Definition of the identified phases

We wish here to identify phases characterized by specific behaviors of nitrate consumption and to determine which processes are responsible for these behaviors. For this purpose, we interpret general tendencies of the results presented in Figure 3a, and we focus on the evolution of nitrate consumption during the experiment for each flow velocity and on the differences observed between the experiments conducted with different flow velocities.

Focusing on the general behavior of nitrate consumption, we observe that the measurements increase with time with small variations around the dashed black curve plotted in Figure 3a until a specific time t^* (denoted here after transition time). The value of this transition time corresponds to the transition between the black and red periods represented in Figure 3b and is evaluated at 460 hours, 266, 300, and 99 hours for the experiments conducted with a flow velocity of 6.2 mm/min, 11, 17, and 35 mm/min, respectively. After these transition times, nitrate consumption clearly differs from the previous general linear behavior, as we observe (i) a “relative” stabilization with small variations for the slower (full blue

curve) and higher (dotted red curve) flow velocities, and (ii) a general decreasing tendency for the intermediate flow velocities (dashed green and dashdot magenta curves). As the variations around the dashed black curve for $t < t^*$ are small in comparison to the divergence from this curve for $t > t^*$, we consider that nitrate consumption can be divided into two phases denoted phase 1 for $t < t^*$ and phase 2 for $t > t^*$.

2. Initiation of degradation processes (phase 1)

In the first phase identified in Figure 3a (denoted phase 1 in Figure 3b), the nitrate consumptions observed for the four flow velocities tend to follow a linear increase in contrast to the large variations observed during the whole experiment. This linear tendency is represented by a dashed black curve in Figure 3a and lasts for the black period represented in Figure 3b. As previously described, the duration of this phase depends on the flow velocity, and lasts, for example, for 92% of the experimental duration for the slower flow velocity and only 19.8% of the experimental duration for the higher flow velocity.

In comparison with the large variations observed during the whole experiment, we consider that nitrate consumptions observed for the different flow velocities present a small range of variation during phase 1. For example, when $t = 67$ h, the experiments conducted with a flow velocity of 6.2 mm/min, 11, 17 and 35 mm/min are in phase 1 and the values of nitrate consumption range from 0.9 to 2.9 mg/L. In opposition, when $t = 187$ h, the experiment conducted with a flow velocity of 35 mm/min is in phase 2 and presents a value of nitrate consumption of 1.2 mg/L, whereas the experiments conducted with a flow velocity of 11 mm/min, 17 and 35 mm/min are in phase 1 and present values of nitrate consumption that range from 4 to 4.8 mg/L.

The previous observations are based on the temporal evolution of nitrate consumption for experiments conducted with several flow velocities. As the residence times within the tubes are flow-velocity dependent, these results might be difficult to interpret. For example, similar values of nitrate consumption correspond to a greater reactivity for a higher flow velocity. In order to take into account the impact of various residence times, we define the nitrate degradation rate $R_{NO_3^-}$ (in mg m^{-2} s^{-1}) as

$$R_{NO_3^-}(t) = \Delta C_{NO_3^-} \times q/S, \quad \textbf{(2)}$$

where q (L/s) is the flow rate within the tube and S (m^2) the reactive tube surface in contact with the water. In addition, as the quantity of water passing through the system until a given time is flow-velocity dependent as well, we define the pore volume number P_{vol} (-) as

$$P_{vol}(t) = t \times q/V, \quad \textbf{(3)}$$

which corresponds to the volume of water used in the system until time t divided by the tube volume V (m^3). In other words, the pore volume number enables us to evaluate the number of tubes that are filled up until a given time for a given flow velocity. Studying the evolution of the nitrate degradation rate $R_{NO_3^-}$ with the pore volume number P_{vol} enables us to compare the reactivity observed for different flow velocities considering similar quantities of water used in the system.

Figure 5a represents the evolution of the nitrate degradation rate $R_{NO_3^-}$ with the number of pore volumes P_{vol} and Figure 5b shows the duration of phase 1 in terms of pore volume numbers. These durations are evaluated by using equation 3 with the transition times t^* previously determined for each flow velocity. It leads to duration of phase 1 in terms of pore volume numbers equal to 126.8, 130, 226.7, and 154 for the flow velocity 6.2 mm/min,

11, 17, and 35 mm/min, respectively. These results show as well that strong variations of the nitrate degradation rate are not observed during phase 1 and are rather observed after this phase. These observations are again relative to the general behavior during the whole experiment, as nitrate degradation rate differs for the flow velocity 35 mm/min from the values observed for the three lower flow velocities. However, these variations are small in comparison to the variations observed during the rest of the experiments. It implies that the consumption (or degradation) rate of nitrates depends mainly on the quantity of water passed through the tubes (i.e., the number of pore volumes) and that flow velocity impacts mainly the final behavior of the reactivity (phase 2). The mass of nitrate consumed per pore volume is thus independent of the residence time.

At the beginning of the experiment biofilm develops as clusters from the millimeter to the centimeter scale (Figure 4a), and then spreads continuously along the tubes (Figure 4b). During this first phase, the increase of the degradation rate with time can therefore be related to biofilm development inside the tubes. As nitrate and organic carbon are present at the tube outlets (where carbon concentration ranges from 6.5 to 21 mg/L), they are in excess in the system and cannot be considered as limiting factors. The factor controlling this first phase for flow-through experiments is thus the bacterial growth rate leading to a total consumption of nitrate for the static experiments.

3. **Stabilization** and decrease (phase 2)

In the second identified phase (phase 2 in Figure 3), the nitrate consumption is characterized by either (i) a “relative” stabilization with small variations for the slower (full blue curve) and higher (dotted red curve) flow velocities, or (ii) a general decreasing tendency for the intermediate flow velocities (dashed green and dashdot magenta curves). Concerning the

fastest velocity v_4, the previously named "relative stabilization" corresponds to a succession of decreases and increases oscillating around a "relative threshold".

As carbon and nitrates (the main reactants) are still in excess at the tube outlets, their availability is not the limiting factor. The nitrate reduction capacity during this phase seems thus to be controlled by the flow velocity that can impact biofilm properties. The following section is dedicated to explaining the experimental observations by relating them to biofilm properties. The two phases previously identified are linked to several steps of the biofilm development with specific flow-dependences.

IV. Linking biofilm properties and reaction processes

From the measurements of nitrate and nitrite concentrations in both static and flow-through experiments, the present section aims to evaluate the biofilm properties and relate them to the observed reaction efficiency.

1. Evaluation of biofilm properties

Cumulative biofilm weight

Since the dynamic of biofilm development is likely important in the reaction rate evolution, we aim to evaluate the dynamic of produced biofilm mass during the experiments. Continuous monitoring and complete quantification of the biofilm were not possible during the experiment due to technical reasons. To counteract this problem, we propose to estimate the biofilm property evolution considering that the production of cells can be calculated using the method of McCarty [1972] in which the quantity of produced mass depends on the electron donor. For example, 0.24 g of cells is produced per gram NO_3-N removed for H_2 [Ergas and Reuss, 2001; Ergas and Rheinheimer, 2004], 0.64 g of cells in the case of sulfur [Sengupta

and Ergas, 2006], and 0.45 g and 1.21 g of cells in the case of methanol and acetic acid, respectively [Hamlin et al., 2008]. Those authors consider that the usual range of heterotrophic denitrification is between 0.6 and 0.9 g of cells produced per gram of NO_3-N removed. In the present study, and for demonstration purposes, we consider the mean value of the previous range, corresponding to 0.75 g of cells produced per gram of NO_3-N removed, or 0.17 g of organic matter produced per gram of nitrate consumed.

Note that the main uncertainty is then about N gasses (N_2, NO) that are produced but not measured (as explained in section 2.4). However, the corresponding reaction given by equation 4 in the case of methanol [Hamlin et al., 2008] shows that, even if a considerable mass of cells can be produced in comparison to the mass of nitrate removed, only a small fraction of nitrogen is assimilated in the cell and most of it is reduced to N_2

$$NO_3^- + 1.08\ CH_3OH + H^+ \rightarrow 0.065\ C_5H_7O_2N + 0.47\ N_2 + 0.75\ CO_2 + 2.44\ H_2O. \quad (4)$$

Assuming that 1 g of consumed nitrate allows the production of 0.17 g of organic matter, we calculate the temporal evolution of the cumulative biofilm weight $\overline{m_{bio}}$ (g) from the NO_3 and NO_2 in and out fluxes as

$$\overline{m_{bio}}(t) = 0.17 \times M_{NO_3^-} \times \overline{n_{NO_3^-}^{bio}}(t) - k_{bio}(t), \quad (5)$$

where $M_{NO_3^-}$ (g/mol) is the molar mass of nitrate, $\overline{n_{NO_3^-}^{bio}}$ (mol) the total number of nitrate moles used for biofilm formation until time t, and k_{bio} (g) a "loss parameter" that represents potential loss of biomass that could be flushed out of the tubes. The number of moles $\overline{n_{NO_3^-}^{bio}}$ in equation 5 is evaluated from the number of consumed nitrate moles $\overline{n_{NO_3^-}^{cons}}$ (mol) and produced nitrite moles $\overline{n_{NO_2^-}^{prod}}$ (mol) as

$$\overline{n_{NO_3^-}^{bio}}(t) = \overline{n_{NO_3^-}^{cons}}(t) - \overline{n_{NO_2^-}^{prod}}(t). \quad (6)$$

Note that equation 6 assumes that the quantity of nitrate used for biofilm formation corresponds to the quantity of consumed nitrate that is not transformed to nitrite. As stated before, it assumes that only a small portion of the consumed nitrate is reduced to gas and that this quantity can be neglected. In addition, the previous formulation considers that biofilm formation is not limited by the availability of carbon, as we observe that this reactant is in excess during the whole experiment.

In equation 6, the molar quantities $\overline{n_{NO_3^-}^{cons}}$ and $\overline{n_{NO_2^-}^{prod}}$ are deduced from nitrate and nitrite concentration measurements. Thus, the total number of nitrate moles used for biofilm formation until time *t* is expressed as follows.

For batch experiments:

$$\overline{n_{NO_3^-}^{bio}}(t) = \left\{ \frac{\left[C_{NO_3^-}^{IN} - C_{NO_3^-}^{OUT}(t)\right]}{M_{NO_3^-}} - \frac{C_{NO_2^-}^{OUT}(t)}{M_{NO_2^-}} \right\} \times V, \quad (7)$$

and for flow-through experiments:

$$\overline{n_{NO_3^-}^{bio}}(t) = \int_0^t \left\{ \frac{\left[C_{NO_3^-}^{IN} - C_{NO_3^-}^{OUT}(\tau)\right]}{M_{NO_3^-}} - \frac{C_{NO_2^-}^{OUT}(\tau)}{M_{NO_2^-}} \right\} \times q \, d\tau, \quad (8)$$

where $C_{NO_3^-}^{IN}$ is the nitrate concentration defined in the previous section, $C_{NO_3^-}^{OUT}(t)$ and $C_{NO_2^-}^{OUT}(t)$ (g/L) are nitrate and nitrite concentrations, respectively, measured at time *t* in the batch volume (for batch experiment) and at the tube outlets (for flow-through experiments), $M_{NO_2^-}$ (g/mol) is the molar mass of nitrite, V (L) is the water volume for the batch experiment and q (L/s) the flow rate for the flow-through experiments.

Figure 6 shows the temporal evolution of biofilm properties characterized by the cumulative biofilm weight $\overline{m_{bio}}$ (in mg). Concerning the differences between batch (large black curve) and flow-through (full blue, dashed green, dashdot magenta and dotted red curves) experiments, we observe that (i) a stronger increase of the biofilm weight is observed for the batch experiment, and (ii) the batch experiment leads to a constant biofilm weight observed in the last part of the large black curve. These observations are related to differences between the experimental setup of the batch and flow-through experiments, where all the nitrates to be consumed are present in the batch volume at the very beginning of the batch experiment, whereas the nitrates are progressively introduced into the system for the flow-through experiments. It implies that the nitrate concentration is higher at the beginning of the batch experiment and that the biofilm weight increases quickly until total consumption of the nitrate present in the batch volume.

Concerning the flow-through experiments, differences are observed for the different flow velocities (Figure 6). For a given time, the biofilm weight increases when increasing the flow velocities for the experiments conducted with the flow velocities v_1, v_2, and v_3. In relation to the results presented in Figure 3, nitrate consumption for these three flow velocities present small differences during phase 1 in contrast to the large differences observed during the rest of the experiment. These small differences are observed for 266 hours, as it is the smallest duration of phase 1 for the flow velocities v_1, v_2, and v_3. As biofilm weight estimates are based on the values of nitrate consumption and flow rate (equation 5-8), the differences observed before this specific time are mainly due to the different flow velocities of these experiments. Knowing that these velocities regulate the quantity of nitrates entering into the system, a higher flow velocity results in a larger biofilm weight, as observed for the flow velocities v_1, v_2, and v_3 from $t = 0$ to $t = 266$ hours. After this specific time, although

nitrate consumption in Figure 3a is higher for the slower velocity, these differences with the other flow velocities are not large enough to modify the previous behavior. Note that the previous observations are not valid for the experiment conducted with the highest velocity v_4, as nitrate consumption in this case differs from the nitrate consumption observed for the three lowest velocities after 100 hours (Figure 3a). We observe then in Figure 6a that the small values of nitrate consumption combined with the high flow velocity v_4 lead to a biofilm weight comparable to the estimate obtained for the flow velocity v_3.

At the end of the slowest experiment, the biofilm has been extracted from the tube and its dry weight evaluated at 1.9 mg, whereas the proposed model leads to a cumulative biofilm weight of 0.62 mg. This difference is likely due to the simplifications of the proposed model where the addition of suspended materials and Extracellular Polymeric Substances are not considered. Uncertainties remain as well concerning the relation linking cells produced per quantity of consumed nitrate and the impact of flow velocity on the reaction stoichiometry. All the previous processes could contribute to the increase of the biofilm weight evaluated by our model. In addition, as the measurement of biofilm by extraction from the tube is destructive, it can be done only once at the end of the experiment. This limitation prevents us from obtaining extensive data on the biofilm properties. However, as previously explained, this experimental setup is the most convenient in order to study the impact of hydraulic properties on reactivity. In addition, the present study aims to conduct a qualitative analysis where we are particularly interested in the relative temporal evolution of the biofilm properties for different flow velocities and in their link to the reaction efficiency. As the proposed model tends to underestimate the biofilm weight, the parameter k_{bio} that represents potential loss of biofilm is set to 0 and we assume that processes such as detachment and decay are negligible in the present study. Regarding the previous assumptions, biofilm

properties such as biomass and thickness are referred and interpreted as cumulative properties along the experimental time.

Cumulative biofilm thickness

For comparison with previous studies, we evaluate the cumulative biofilm thickness b_{bio} by considering that biofilm forms a uniform cylinder stuck on the tube wall. The cumulative biofilm thickness b_{bio} is defined as

$$b_{bio} = R - \sqrt{R^2 - {V_{bio}}/{\pi L}}, \quad (9)$$

where R is the radius of the tube, L the tube length, and V_{bio} the biofilm volume. This volume is deduced from the cumulative biofilm mass $\overline{m_{bio}}$ (equation 5) assuming a biofilm mass density of 10 mg/cm^3 [Williamson and McCarty, 1976]. In order to obtain comparable results, the same geometry is assumed for static and flow-through experiments. Note that biofilm thickness gives the same qualitative information as the biofilm weight and is introduced here only for an easier comparison with existing studies.

As tube experiments are conducted for several flow velocities, the temporal evolution of biofilm is potentially impacted by both the effect of flow on biofilm structure and the mass of nutrient injected into the system over time. In order to focus on the interactions between flow and biofilm-structure properties, we study the biofilm evolution with the quantity of nutrient input N_{input} (g). For batch experiments, N_{input} corresponds to the mass of nitrate present in the tank at the beginning of the experiment and is defined as

$$N_{input} = C_{NO_3^-}^{IN} \times V. \quad (10)$$

For the flow-through experiments, $N_{input}(t)$ corresponds to the mass of nitrate introduced into the system until time t and is defined as

$$N_{input}(t) = C_{NO_3^-}^{IN} \times q \times t. \quad (11)$$

Figure 7 shows the evolution of the biofilm properties (characterized here by the cumulative biofilm thickness b_{bio}) with the quantity of nutrient input N_{input}. The batch experiment (large black curve) leads to a fast consumption of nutrient because the small initial quantity of nutrient is not enriched by new inputs. Concerning the flow-through experiments, the presented results show that increasing the flow velocity leads to (i) smaller values of the biofilm thickness per nutrient input unit, and (ii) a slower evolution of the biofilm growth along the quantity of injected nutrient. It implies that fast velocities result in a thinner (or less dense) "effective" biofilm per nutrient input unit, where "effective" means that the biofilm is assumed to be homogeneous and of the same density for all experiments. This biofilm thickness per nutrient input unit can also be interpreted as a "potential" thickness, as its estimate does not take into account possible erosion and/or detachment processes. Note that the previous observations are valid for the evolution of the biofilm thickness along the quantity of nutrient injected into the system and not along the experimental time.

By relating biofilm growth to the nitrate transformation rate, the next section aims to characterize how the evolution of biofilm properties is related to the flow velocity and how the flow velocity impacts the reaction efficiency.

4. Linking biofilm growth and nitrate transformation

In order to illustrate the flow-dependent heterogeneity of biofilm structures and its potential role on nitrate transformation, we calculate the rate of nitrate transformation V_{trans} (mg m^{-2} s^{-1}) and compare it to our estimate of biofilm thickness.

For the batch experiment, V_{trans} is defined as

$$V_{trans}(t) = \frac{\Delta C_{NO_3^-}^{bio}}{\Delta t} \times \frac{V}{S} \quad (12)$$

where $\Delta C_{NO_3^-}^{bio}$ (g/L) is the concentration of nitrate transformed in biofilm during the time interval Δt and S is the reactive PVC surface. The value of $\Delta C_{NO_3^-}^{bio}$ at time t_i is evaluated by the following expression for the batch experiment:

$$\Delta C_{NO_3^-}^{bio}(t_i) = \left[n_{NO_3^-}^{bio}(t_i) - n_{NO_3^-}^{bio}(t_{i-1})\right] \times M_{NO_3^-} \quad (13)$$

where $n_{NO_3^-}^{bio}(t_i)$ (mol/L) is the number of moles transformed in biofilm per unit of volume until time t_i and is expressed as

$$n_{NO_3^-}^{bio}(t_i) = \frac{C_{NO_3^-}^{IN} - C_{NO_3^-}^{OUT}(t_i)}{M_{NO_3^-}} - \frac{C_{NO_2^-}^{OUT}(t_i)}{M_{NO_2^-}}. \quad (14)$$

For the flow-through experiments, the interval time Δt of expression 12 is set to the time required to travel along the tube by advection (from its inlet to its outlet) and leads to the following expression

$$V_{trans}(t) = \Delta C_{NO_3^-}^{bio} \times \frac{q}{S} \quad (15)$$

where $\Delta C_{NO_3^-}^{bio}$ is the concentration of nitrate contributing to biofilm formation during the interval time Δt. The concentration $\Delta C_{NO_3^-}^{bio}$ in equation 15 is expressed as

$$\Delta C_{NO_3^-}^{bio}(t_i) = \left[n_{NO_3^-}^{bio}(t_i) - n_{NO_3^-}^{bio}(t_0)\right] \times M_{NO_3^-} \quad (16)$$

where $n_{NO_3^-}^{bio}(t_i)$ and $n_{NO_3^-}^{bio}(t_0)$ are defined by expression 14 with $n_{NO_3^-}^{bio}(t_0)$ the value at the tube inlet. Note that the rate of nitrate transformation (equations 12 and 15) and nitrate degradation rate (equation 2) differ, as the first one considers only the nitrate contributing to biofilm growth (assimilation) and the second one considers all the nitrate consumed during the experiment (reduction).

Figure 8 shows the evolution of the nitrate transformation rate V_{trans} (equations 12 and 15) as a function of our estimate of the cumulative biofilm thickness b_{bio} (equation 9) for the batch (black curve) and flow-through experiments (full blue, dashed green, dashdot magenta and dotted red curves). For the batch experiment, the nitrate transformation rate is characterized by (i) a strong increase when the biofilm thickness evolves from 0 to 8.8 μm, and (ii) a strong decrease when the biofilm thickness is larger than 8.8 μm. As expected in this case, biofilm growth is (i) first fast and not limited by nitrate concentration, and (ii) then limited by nutrient availability, as the total quantity of nitrate is consumed at the end of the experiment.

Results presented in Figure 8 show that the very beginning of the flow-through experiments is characterized by a similar strong linear increase of the nitrate transformation rate (dashed black line). The nitrate transformation rate differs from the previous behavior when the biofilm thickness reaches the values of 0.16 and 0.41 μm for the flow-through

experiments v_1 and v_2, respectively, and the value of 1 μm for the flow-through experiments v_3 and v_4.

After the previously described linear increase, the nitrate transformation rate associated with the slowest flow velocity v_1 follows two distinguished behaviors. When the biofilm thickness is between 0.16 and 4.4 μm, the superposition of the large black and full blue curves shows small differences of the nitrate transformation rate for the batch experiment and flow-through experiment v_1. When the biofilm thickness is larger than 4.4 μm, the behavior of these two experiments differs and the nitrate transformation rate is characterized by a relative stabilization for the flow experiment v_1.

Increasing the flow velocity from v_1 to v_2 implies that the initial linear increase of the nitrate transformation rate is observed until the biofilm thickness reaches the value of 0.41 μm (instead of 0.16 μm for the flow velocity v_1). When the biofilm thickness is larger than 0.41 μm, the flow experiment v_2 leads to a relative stabilization of the nitrate transformation rate characterized by small variations in comparison to the initial linear increase.

Finally, the flow experiments conducted with the two fastest flow velocities v_3 and v_4 lead to comparable results. In both cases, the behavior of the nitrate transformation rate differs from the initial linear increase when the biofilm thickness reaches the value of 1 μm. When the biofilm thickness is larger than 1 μm, the nitrate transformation rate is characterized by a series of strong variations that oscillate around a similar threshold value.

V. Discussion

The evolution of the nitrate transformation rate V_{trans} with the biofilm thickness b_{bio} presented in Figure 8 shows different behaviors between the batch and flow-through

experiments and between the flow-through experiments conducted with different flow velocities. These behaviors are described in section 4.2 in terms of experimental-setup and flow-velocity impact on reaction efficiency. In the present section, we wish to relate the previous observations to the evolution of the biofilm properties along the experiment by proposing several scenarios of the flow-velocity impact on these properties. These scenarios are deduced by (i) determining under which conditions the presence of flow impacts nitrate transformation rate, (ii) evaluating the impact of flow velocity on denitrification efficiency and stability, and (iii) discussing the proposed evolution of the biofilm properties in relation to existing studies.

Impact of the presence of flow on nitrate transformation rate

The results presented in Figure 8 are used here to identify under which conditions the presence of flow impacts nitrate transformation rate. For this purpose, we focus on the two following aspects of the evolution of V_{trans} with b_{bio}: (i) the similar linear increase observed for a very short time at the beginning of the flow-through experiments, and (ii) the similarities and differences observed between the flow-through and batch experiments.

When the biofilm thickness is smaller than 0.16 μm, the flow-through experiments show a similar behavior that seems not to depend on the flow velocity. Although additional data are required to characterize this short period, this behavior might be due to a phenomenon that initiates the reactive process, such as attachment of cells by adsorption on the tube walls, which is not flow-velocity dependent for the studied range of velocities.

After this first short-term period, the nitrate transformation rate for the flow-through experiment v_1 and the batch experiment presents small differences until that the biofilm thickness reaches 4.51 μm. Considering the batch experiment as a reference experiment

without flow, it shows that the hydraulic conditions of the flow-through experiment v_1 do not impact the reaction efficiency when the biofilm thickness is between 0.16 and 4.51 μm. In other words, the flow velocity v_1 is most likely too small to modify the structural properties of the biofilm for this range of values of the biofilm thickness. In comparison, the relationship between V_{trans} and b_{bio} for the three fastest flow-through experiments (v_2, v_3 and v_4) clearly differs from the batch experiment. In these cases, the flow velocities may be high enough to impact the biofilm properties during the whole experiment.

Impact of flow velocity on reaction efficiency

A strong linear increase of the nitrate transformation rate with biofilm growth is observed at the beginning of the flow-through experiments. This linear increase is represented by a dashed black curve in Figure 8 and is observed until the biofilm thickness reaches 0.16 μm for the flow velocity v_1, 0.41 μm for the flow velocity v_2, and 1 μm for the flow velocities v_3 and v_4. This fast evolution of the nitrate transformation rate may characterize a fast modification of the biofilm/fluid reactive contact area while the biofilm thickness is smaller than a flow-velocity dependent value. As the nitrate transformation rate increases when increasing the flow velocity during this period, larger values of flow velocity may optimize the reaction efficiency.

In relation to previous studies, it has been demonstrated that hydraulic constraints can imply an increase of the biofilm height [Hornemann et al., 2009] due to the presence of secondary velocities that are perpendicular to the deposit surface and that generate an upward shear force in the downstream side of the biofilm [Vo and Heys, 2011]. It results in a higher and heterogeneous biofilm structure that optimizes the biofilm/fluid contact area and thus the efficiency of the denitrification process. In addition, it has been demonstrated that applying

555 fast advective flows parallel to the deposit surface leads to heterogeneous deposits of bacteria
556 along the tube surface [Yu et al., 1999]. This phenomenon results in the formation of patch
557 structures that have been observed during the experiments (Figure 4a) and where the
558 biofilm/fluid contact area is optimized in comparison to continuous structures.

559 It is important to notice that these conclusions are in contradiction with some previous
560 studies showing that fluid shear tends to compress the biofilm towards the surface [Picioreanu
561 et al., 2001; van Loosdrecht et al., 2002; Wanner et al., 1995]. However, the biofilm models
562 and experiments of these studies are based on assumptions that differ from our experiment,
563 such as homogeneous and isotropic biofilm assumption [Picioreanu et al., 2001] or
564 experimental conditions where flow is applied to a biofilm grown without flow [Wanner et
565 al., 1995]. This demonstrates the complexity of the relationship between biofilm properties
566 and hydrodynamic parameters, the importance of model assumptions and experimental
567 conditions, and the critical differences of biofilm properties when the biofilm grows under
568 static or flow-through conditions.

569 ***Impact of flow velocity on reaction stabilization***

570 Whereas the flow-through experiment v_1 and the batch experiment present small differences
571 when the biofilm thickness is smaller than 4.51 μm, the nitrate transformation rate of these
572 experiments differs for larger values of the biofilm thickness. For these values (larger than
573 4.51 μm), V_{trans} shows a relative stabilization for the flow-through experiment v_1 whereas it
574 keeps increasing for the batch experiment. From these observations, it seems that the
575 hydraulic conditions of the flow-through experiment v_1 lead to biofilm production/loss
576 equilibrium driven by processes such as decay and erosion for larger values of the biofilm
577 thickness.

578 An important change of behaviors is also observed for the flow-through experiments
579 v_2, v_3, and v_4. After the linear increase observed at the beginning of the experiment (black
580 dash curve), the nitrate transformation rate oscillates around the threshold value reached when
581 the biofilm thickness is equal to 0.44 μm for the flow velocity v_2 and 1 μm for the flow
582 velocities v_3 and v_4. The observed successions of increase/decrease cycles of the nitrate
583 transformation rate may characterize repeated variations of the biofilm/fluid reactive contact
584 area, and thus of the biofilm structural properties. Increasing the flow velocity from v_2 to v_3
585 implies that (i) the transition between the linear increase and the relative stabilization is
586 observed for a larger value of the biofilm thickness, (ii) the nitrate transformation rate
587 oscillates around a larger threshold value, and (iii) the variations of the nitrate transformation
588 rate around this threshold value are larger (which is observed as well when increasing the
589 flow velocity from v_3 to v_4).

590 The transition from a linear increase to a relative stabilization starts by a slow decrease
591 of the nitrate transformation rate. This decrease is observed when the biofilm thickness
592 evolves from 1.4 to 3.2 μm for the flow velocities v_3 and v_4 and might characterize a
593 progressive variation of the biofilm structural properties from an optimal configuration to a
594 less reactive configuration. The transition from patches (Figure 4a) to continuous structures
595 (Figure 4b) observed during the experiments is characteristic of the previous behavior where
596 the patch structures optimize the biofilm/fluid contact area (and thus the reactivity) in
597 comparison to continuous structures. In addition, the transition from the first to the second
598 kind of structures might occur progressively with new deposits and/or bacterial growth that
599 fill the spaces between patches.

600 The large oscillations of the nitrate transformation rate observed for the flow velocities
601 v_3 and v_4 may characterize fast and important variations of the biofilm structural properties

due to flow-dependent phenomena such as detachment and reattachment. These experiments correspond to hydraulic conditions with fast flow velocities that can imply a strong heterogeneity of the structures due to upward shear forces and heterogeneous deposits (as explained in the previous section). In relation to previous studies, it has been shown that the formation of heterogeneous structures implies the presence of protuberances on the biofilm surface where microorganisms grow faster and form tower-like colonies [Picioreanu et al., 1998]. It leads to the presence of cavities where nutrients are not easily accessible and enhances the fragility of the biofilm, and thus potential detachment. In addition, for strong shear stress (correlated to fast flows), the potential detachment promotes biofilm spatial heterogeneity by reattachment [Stewart, 1993]. The observed succession of decreases and increases might thus be due to detachments and reattachments related to a strong heterogeneity of the biofilm structures.

VI. Conclusion

The presented experiment and analytical framework aim to characterize biochemical reactivity in the case of mobile/immobile electron acceptor/donor under flow-through conditions to assess the influence of flow velocity on biologically constrained reaction rates. This is done through an original experiment where nitrate-rich water passes continuously through plastic tubes at several flow velocities (from 6.2 to 35 mm/min). Flow velocity appears to be a key factor for reaction efficiency and stability as experiments conducted with the largest flow velocities are characterized by a fast increase of the reactivity rate until reaching a threshold where strong oscillations are observed. This behavior may characterize an optimization of the biofilm/fluid reactive contact area followed by equilibrium between bacteria development and flow impact on the biofilm structures subject to decay/detachment

phenomena. In opposition, the same experiment conducted with a small flow velocity leads to a slow increase of the reactivity rate until reaching a stable threshold value.

The different behaviors observed between batch and flow-through experiments show the relevance of flow-through experiments for the understanding and characterization of biogeochemical processes in natural media. The presented flow-through experiments demonstrate that the presence of flow impacts the reactivity-rate behavior at different steps of the biofilm development with step-dependent effects of the flow intensity. In natural environments characterized by a broad range of flow velocities, such as soils with macropores or fractured aquifers, the resulting heterogeneous reaction rates might impact the global reactivity of the site. In addition, flow-through conditions related to long-term pumping for water exploitation seem to have an impact on biogeochemical reactivity as observed in the Ploemeur site [Tarits et al., 2006] by enhancing the long-term reactivity at the site scale. For fractured media, most of the denitrification process should occur within the fractures, as they are opened channels favorable to microbial development and nutrient (i.e. nitrates) circulation [Johnson et al., 1998] where the electron donor, such as pyrite, is present as a solid phase.

This study presents an interesting experiment to characterize the influence of flow velocity on biogeochemical reactions where the impact of flow velocity on reactivity is demonstrated. We further propose a framework for its interpretation. Unfortunately it was not possible to continuously monitor and characterize the biofilm due to technical constraints. Future works should include a detailed biofilm characterization and measurements of the biomass flowing out of the tubes. However, this study provides interesting insights on the interest of flow-through experiments over static experiments as well as on the complexity of reactivity in flow-through conditions. In addition, it improves our understanding of heterogeneous and velocity-dependent reactivity in both porous and fractured media.

Although this experiment was designed with the example of denitrification in synthetic conditions, observations and conclusions should be easily transposable to other applications.

Acknowledgements

The French National Research Agency ANR is acknowledged for its financial funding through the MOHINI project (ANR-07-VULN-008) as well as The National Observatory for Research in Environment H+ (SNO H +) for the support of the field data investigations. Financial support was also provided by the EU-RDF INTERREG IVA France (Channel) - England program (Climawat project).

Figures

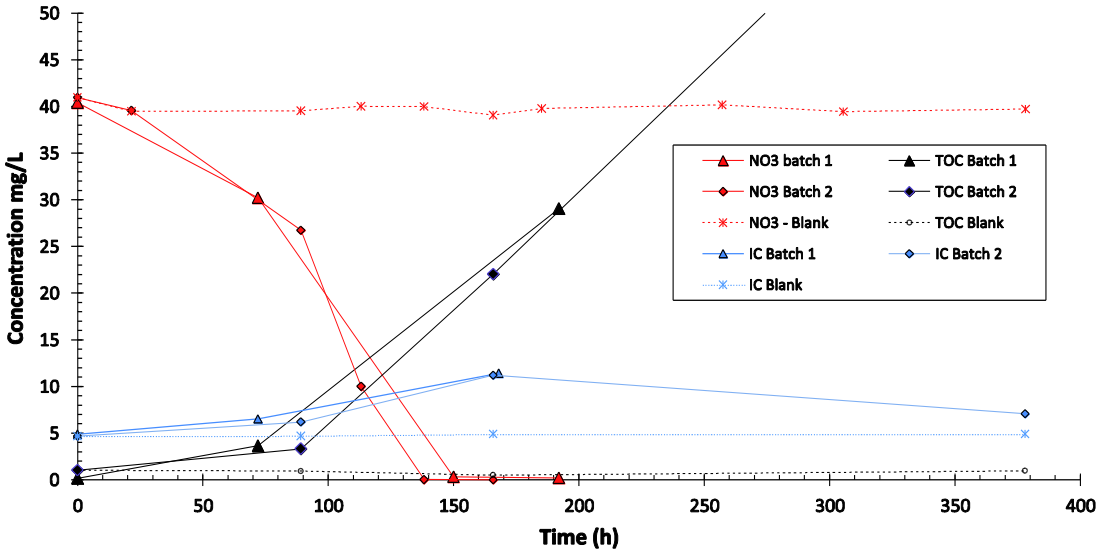

Figure 1 – Evolution of nitrates, total organic carbon (TOC), and inorganic carbon (IC) for batch experiments.

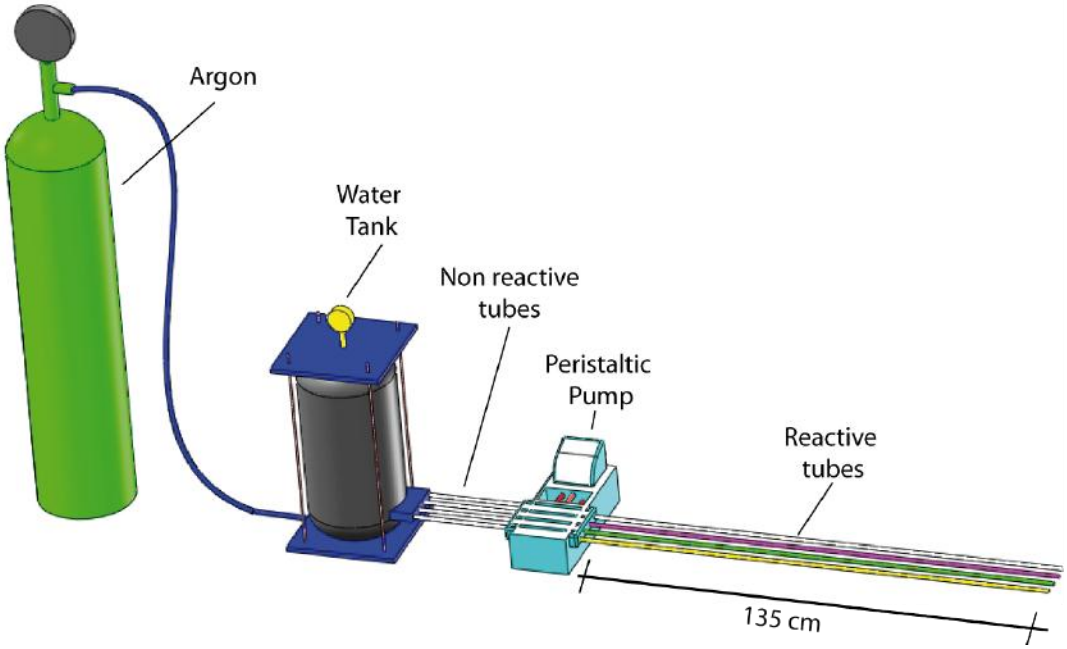

Figure 2 - Schematic representation of the experimental setup .The water is maintained under an argon atmosphere in a tank. The water passes through non-reactive tubes from the tank to the peristaltic pump and then through reactive tubes at different velocities. For each experiment, a non-reactive tube of the same length is used in parallel to assess the inlet concentration.

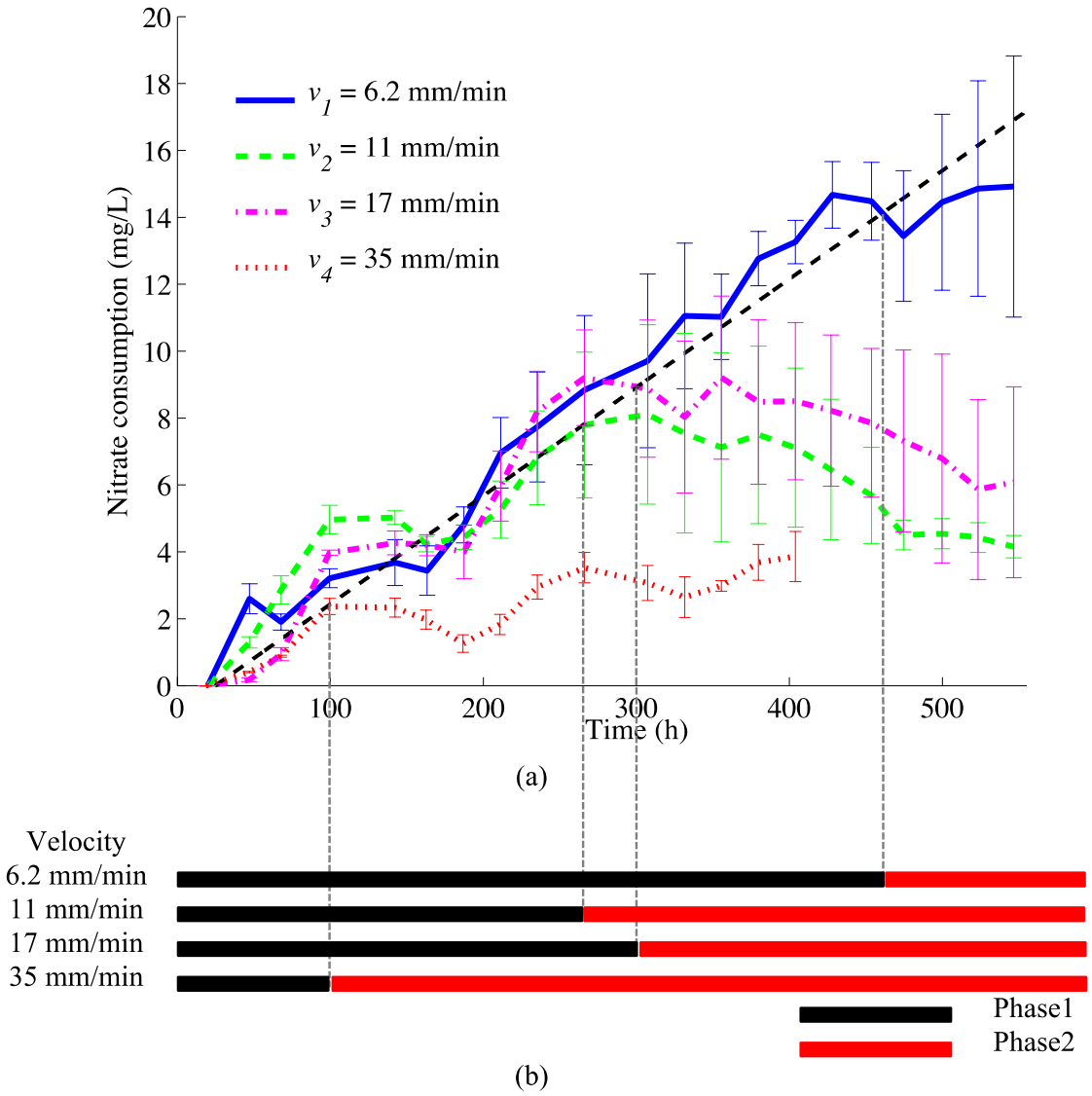

669

670 **Figure 3 – (a) Temporal evolution of the nitrate consumption $\Delta C_{NO_3^-}(t)$ (mg/L) for the**
671 **flow-through experiments conducted with the flow velocities v_1 (full blue curve), v_2**
672 **(dashed green curve), v_3 (dashdot magenta curve), and v_4 (dotted red curve). The**
673 **presented values are the averages of 3 replicates where error bars represent the mean**
674 **square deviation. (b) Duration in hours of phase 1 and phase 2.**

675

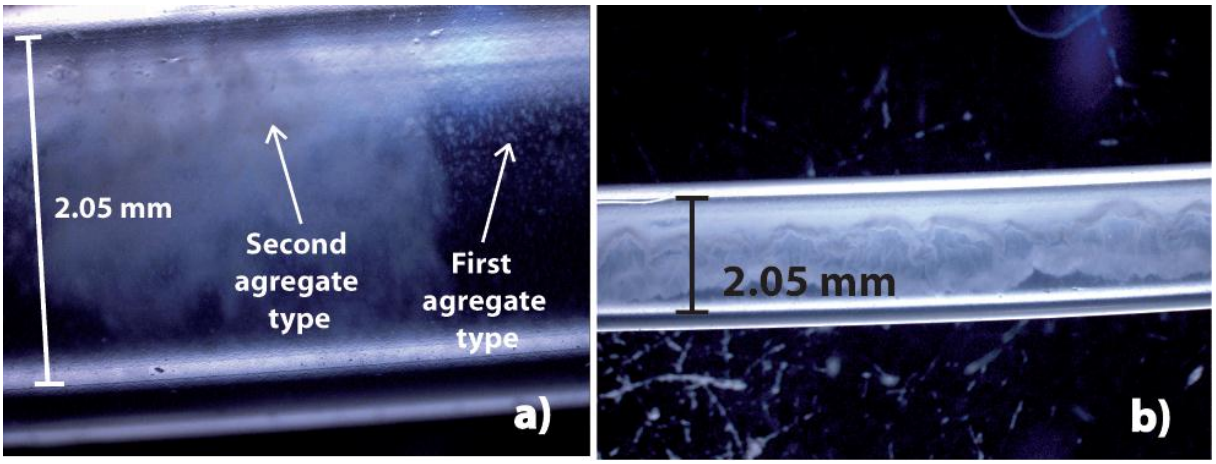

Figure 4 - Biofilm development in the tubes as (a) millimeter and centimeter long clusters, and (b) continuous biofilm.

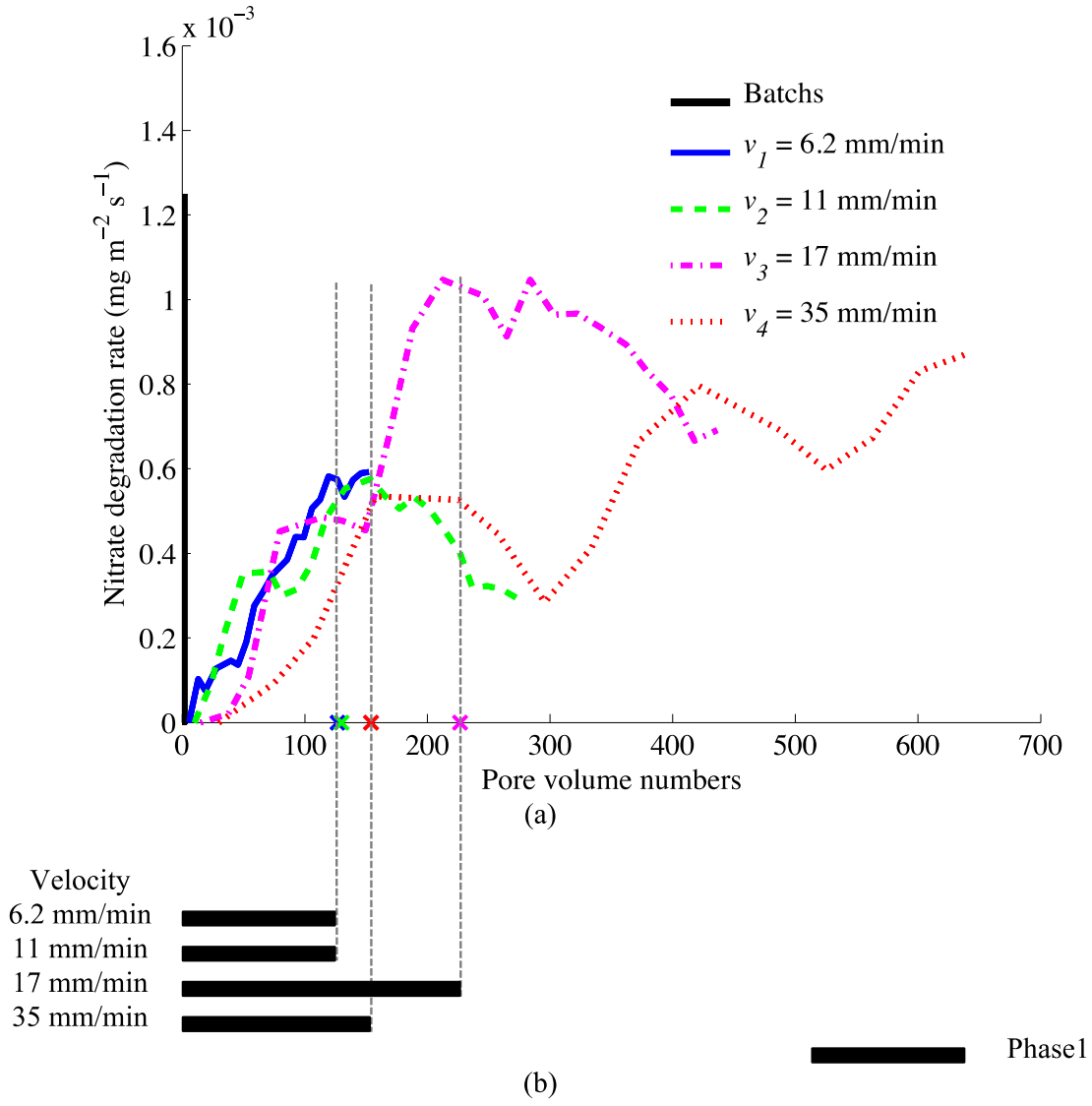

680

681 **Figure 5 – (a) Nitrate degradation rate versus the number of pore volumes for the batch**

682 **(black curve) and tube experiments conducted with the flow velocities v_1 (full blue**

683 **curve), v_2 (dashed green curve), v_3 (dashdot magenta curve), and v_4 (dotted red curve).**

684 **(b) Duration of phase 1 expressed in pore volume numbers.**

685

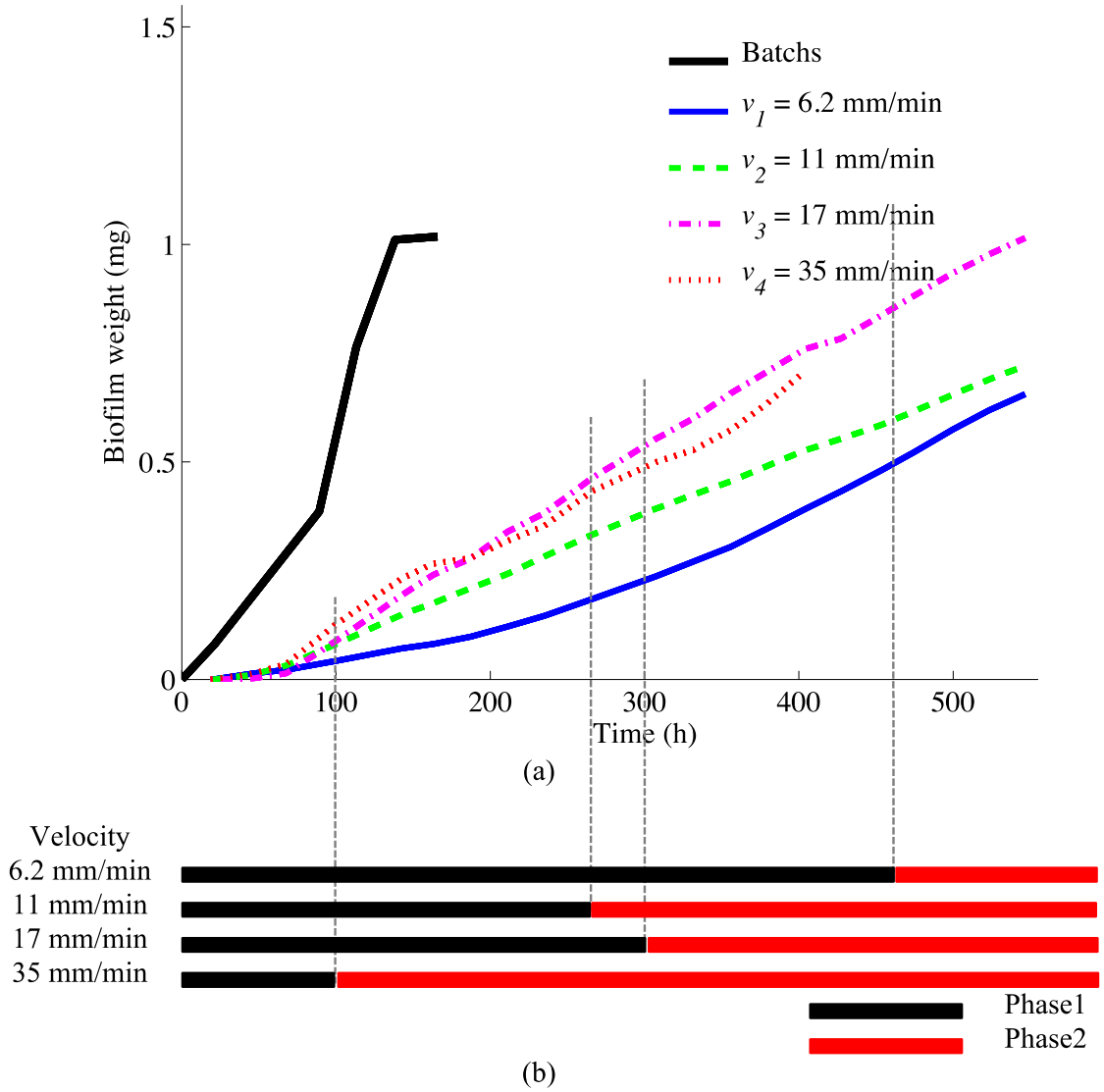

686

687 **Figure 6 – (a) Temporal evolution of the total biofilm weight $\overline{m_{bio}}$ (mg) for the batch**

688 **(black curve) and tube experiments conducted with the flow velocities v_1 (full blue**

689 **curve), v_2 (dashed green curve), v_3 (dashdot magenta curve), and v_4 (dotted red curve).**

690 **(b) Duration in hours of phase 1 and phase 2.**

691

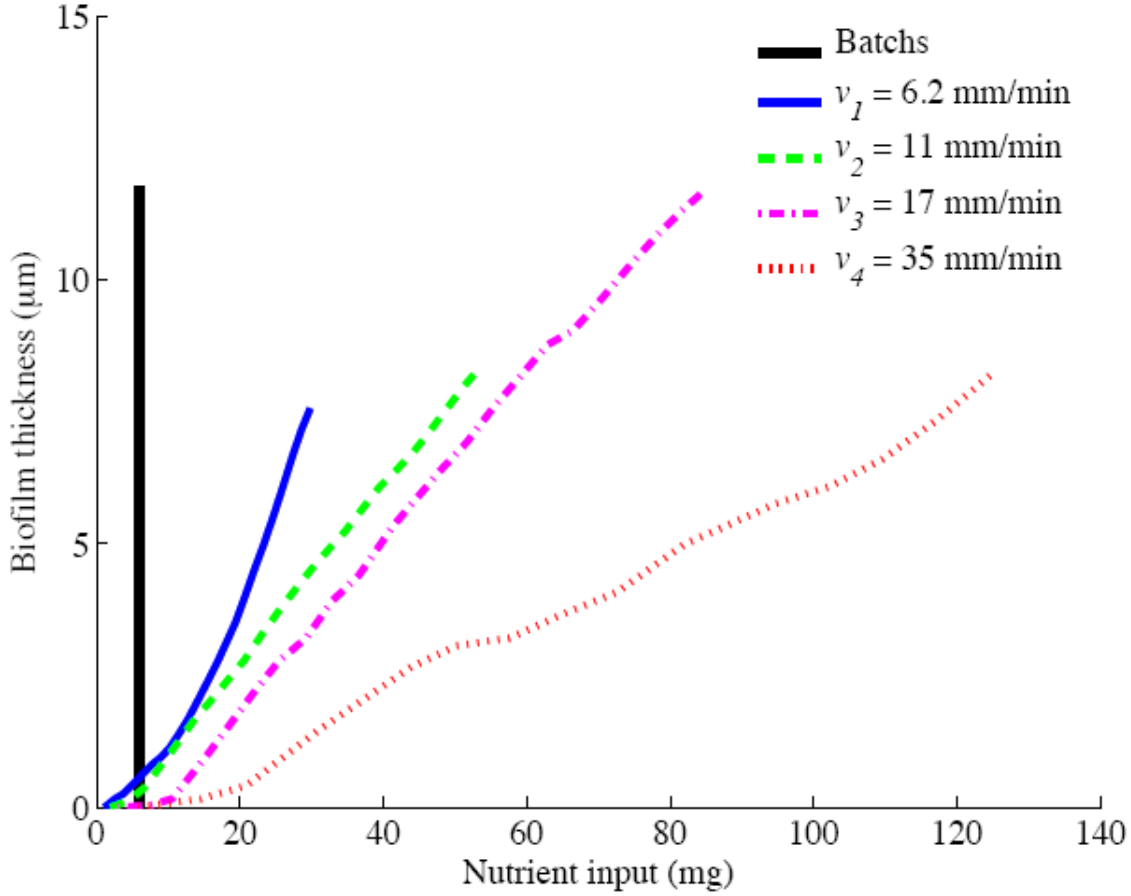

Figure 7 – Evolution of the biofilm thickness b_{bio} (µm) with the nutrient input N_{input} (mg) for the batch (black curve) and tube experiments conducted with the flow velocities v_1 (full blue curve), v_2 (dashed green curve), v_3 (dashdot magenta curve), and v_4 (dotted red curve).

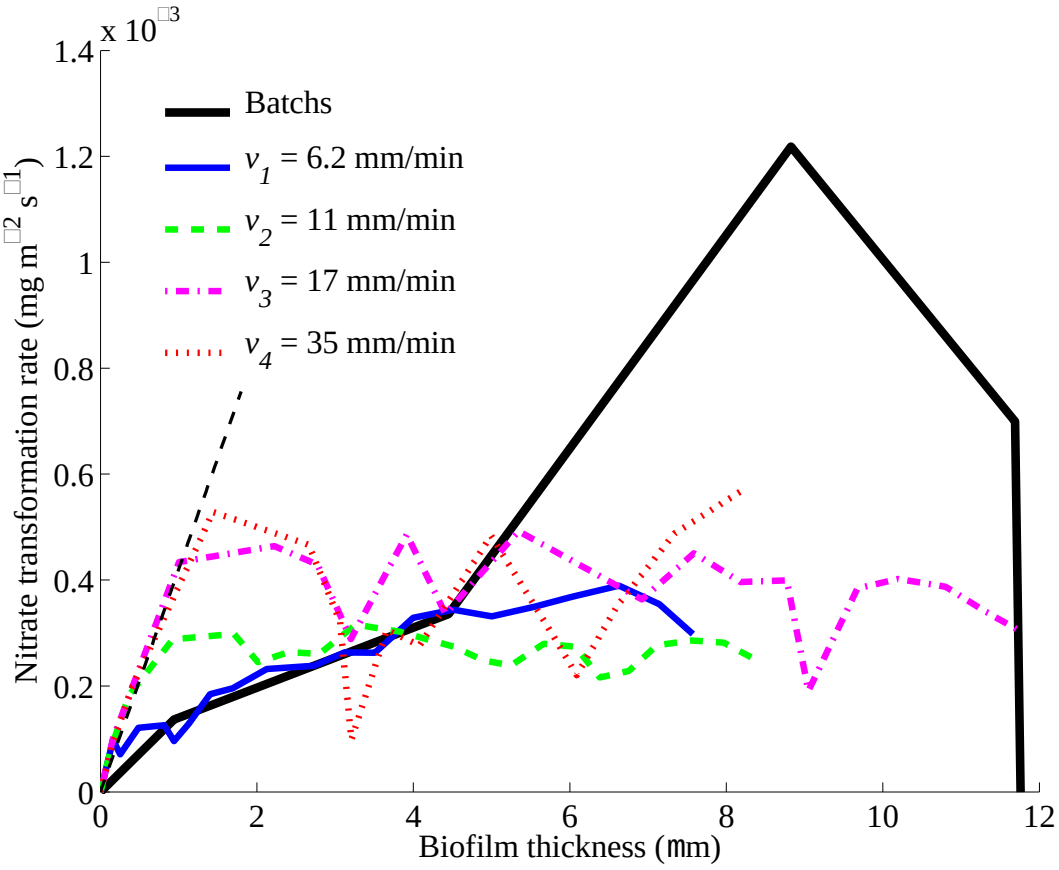

698

699 **Figure 8 - Evolution of the nitrate transformation rate V_{trans} (mg m^{-2} s^{-1}) with the**
700 **biofilm thickness b_{bio} (µm) for the batch (black curve) and tube experiments conducted**
701 **with the flow velocities v_1 (full blue curve), v_2 (dashed green curve), v_3 (dashdot**
702 **magenta curve), and v_4 (dotted red curve).**

703

704 **References**

705 Ayraud, V., Aquilina, L., Pauwels, H., Labasque, T., Pierson-Wickmann, A.-C., Aquilina, A.-
706 M., and Gallat, G. (2006), Physical, biogeochemical and isotopic processes related to
707 heterogeneity of a shallow crystalline rock aquifer, *Biogeochemistry*, 81, 331-347
708 Bekins, B. (2000), Preface - Groundwater and microbial processes, *Hydrogeology Journal*, 8,
709 2-3
710 Beyenal, H. and Lewandowski, Z. (2000), Combined effect of substrate concentration and
711 flow velocity on effective diffusivity in biofilms, *Water Research*, 34, 528-538
712 Boisson, A., de Anna, P., Bour, O., Borgne, T. L., Labasque, T., and Aquilina, L. (2013),
713 Reaction chain modeling of denitrification reactions during a push--pull test, *Journal of*
714 *Contaminant Hydrology*, 148, 1-11
715 Bougon, N., Aquilina, L., Briand, M. P., Coedel, S., and Vandenkoornhuyse, P. (2009),
716 Influence of hydrological fluxes on the structure of nitrate-reducing bacteria communities in a
717 peatland, *Soil Biology and Biochemistry*, 41, 1289-1300
718 Characklis, W. G. (1981), Fouling biofilm development: A process analysis, *Biotechnology*
719 *and Bioengineering*, 23, 1923-1960
720 Clément, J.-C., Aquilina, L., Bour, O., Plaine, K., Burt, T. P., and Pinay, G. (2003),
721 Hydrological flowpaths and nitrate removal rates within a riparian floodplain along a fourth-
722 order stream in Brittany (France), *Hydrological Processes*, 17, 1177-1195
723 Cunningham, A. B., Characklis, W. G., Abedeen, F., and Crawford, D. (1991), Influence of
724 biofilm accumulation on porous media hydrodynamics, *Environmental Science &*
725 *Technology*, 25, 1305-1311
726 De Beer, D., Stoodley, P., and Lewandowski, Z. (1996), Liquid flow and mass transport in
727 heterogeneous biofilms, *Water Research*, 30, 2761-2765

728 Donlan, R. (2002), Biofilms: Microbial life on surfaces, *Emerging Infectious Diseases*, 8,
729 881-890
730 Ergas, S. and Reuss, A. (2001), Hydrogenotrophic denitrification of drinking water using a
731 hollow fibre membrane bioreactor, *Journal of Water Supply: Research &Technology - AQUA*,
732 50, 161-171
733 Ergas, S. J. and Rheinheimer, D. E. (2004), Drinking water denitrification using a membrane
734 bioreactor, *Water Research*, 38, 3225-3232
735 Garny, K., Neu, T. R., and Horn, H. (2009), Sloughing and limited substrate conditions
736 trigger filamentous growth in heterotrophic biofilms-Measurements in flow-through tube
737 reactor, *Chemical Engineering Science*, 64, 2723-2732
738 Hamlin, H. J., Michaels, J. T., Beaulaton, C. M., Graham, W. F., Dutt, W., Steinbach, P.,
739 Losordo, T. M., Schrader, K. K., and Main, K. L. (2008), Comparing denitrification rates and
740 carbon sources in commercial scale upflow denitrification biological filters in aquaculture,
741 *Aquacultural Engineering*, 38, 79-92
742 Hiscock, K. M., Lloyd, J. W., and Lerner, D. N. (1991), Review of natural and artificial
743 denitrification of groundwater, *Water Research*, 25, 1099-1111
744 Hornemann, J. A., Codd, S. L., Fell, R. J., Stewart, P. S., and Seymour, J. D. (2009),
745 Secondary flow mixing due to biofilm growth in capillaries of varying dimensions,
746 *Biotechnology and Bioengineering*, 103, 353-360
747 Istok, J. D., Park, M. M., Peacock, A. D., Oostrom, M., and Wietsma, T. W. (2007), An
748 experimental investigation of nitrogen gas produced during denitrification, *Ground Water*, 45,
749 461-467
750 Jiménez-Martínez, J., Longuevergne, L., Le Borgne, T., Davy, P., Russian, A., and Bour, O.
751 (2013), Temporal and spatial scaling of hydraulic response to recharge in fractured aquifers:

752 Insights from a frequency domain analysis, *Water Resources Research*, 49, 3007-3023
753 Johnson, A. C., Hughes, C. D., Williams, R. J., and Chilton, P. J. (1998), Potential for aerobic
754 isoproturon biodegradation and sorption in the unsaturated and saturated zones of a chalk
755 aquifer, *Journal of Contaminant Hydrology*, 30, 281-297
756 Khan, I. A. and Spalding, R. F. (2004), Enhanced in situ denitrification for a municipal well,
757 *Water Research*, 38, 3382-3388
758 Kornaros, M. and Lyberatos, G. (1997), Kinetics of aerobic growth of a denitrifying
759 bacterium, Pseudomonas denitrificans, in the presence of nitrates and/or nitrites, *Water*
760 *Research*, 31, 479-488
761 Korom, S. F. (1992), Natural denitrification in the saturated zone: A review, *Water Resources*
762 *Research*, 28, 1657-1668
763 Lau, Y. L. and Liu, D. (1993), Effect of flow rate on biofilm accumulation in open channels,
764 *Water Research*, 27, 355-360
765 Leray, S., de Dreuzy, J.-R., Bour, O., Labasque, T., and Aquilina, L. (2012), Contribution of
766 age data to the characterization of complex aquifers, *Journal of Hydrology*, 464-465, 54-68
767 Lewandowski, Z., Beyenal, H., Myers, J., and Stookey, D. (2007), The effect of detachment
768 on biofilm structure and activity: the oscillating pattern of biofilm accumulation, *Water*
769 *Science and Technology*, 55, 429-436
770 Li, L., Steefel, C. I., Kowalsky, M. B., Englert, A., and Hubbard, S. S. (2010), Effects of
771 physical and geochemical heterogeneities on mineral transformation and biomass
772 accumulation during biostimulation experiments at Rifle, Colorado, *Journal of Contaminant*
773 *Hydrology*, 112, 45-63
774 Marazioti, C., Kornaros, M., and Lyberatos, G. (2003), Kinetic modeling of a mixed culture
775 of Pseudomonas Denitrificans and Bacillus subtilis under aerobic and anoxic operating

776 conditions, *Water Research*, 37, 1239-1251
777 McCarty, P. L. (1972), *Stoichiometry of Biological Reactions*, Stanford University. Dept. of
778 Civil Engineering
779 Mohee, R., Unmar, G. D., Mudhoo, A., and Khadoo, P. (2008), Biodegradability of
780 biodegradable/degradable plastic materials under aerobic and anaerobic conditions, *Waste*
781 *Management*, 28, 1624-1629
782 Picioreanu, C., van Loosdrecht, M., and Heijnen, J. (1998), Mathematical modeling of biofilm
783 structure with a hybrid differential-discrete cellular automaton approach, *Biotechnology and*
784 *Bioengineering*, 58, 101-116
785 Picioreanu, C., van Loosdrecht, M., and Heijnen, J. (2001), Two-dimensional model of
786 biofilm detachment caused by internal stress from liquid flow, *Biotechnology and*
787 *Bioengineering*, 72, 205-218
788 Ruelleu, S., Moreau, F., Bour, O., Gapais, D., and Martelet, G. (2010), Impact of gently
789 dipping discontinuities on basement aquifer recharge: An example from Ploemeur (Brittany,
790 France), *Journal of Applied Geophysics*, 70, 161-168
791 Sengupta, S. and Ergas, S. (2006), Autotrophic biological denitrification with elemental sulfur
792 or hydrogen for complete removal of nitrate-nitrogen from a septic system wastewater,
793 *NOAA/UNH Cooperative Institute for Coastal and Estuarine Environmental Technology*
794 *(CICEET)*
795 Shah, A. A., Hasan, F., Hameed, A., and Ahmed, S. (2008), Biological degradation of
796 plastics: A comprehensive review, *Biotechnology Advances*, 26, 246-265
797 Singh, R., Paul, D., and Jain, R. K. (2006), Biofilms: implications in bioremediation, *Trends*
798 *in Microbiology*, 14, 389-397
799 Sinke, A. J. C., Dury, O., and Zobrist, J. (1998), Effects of a fluctuating water table: column

study on redox dynamics and fate of some organic pollutants, *Journal of Contaminant Hydrology*, 33, 231-246

Spalding, R. and Exner, M. (1993), Occurrence of Nitrate in Groundwater - a Review, *Journal of Environmental Quality*, 22, 392-402

Stewart, P. S. (1993), A model of biofilm detachment, *Biotechnology and Bioengineering*, 41, 111-117

Stoodley, P., De Beer, D., and Lewandowski, Z. (1994), Liquid Flow in Biofilm Systems, *Applied and Environmental Microbiology*, 60, 2711-2716

Sturman, P. J., Stewart, P. S., Cunningham, A. B., Bouwer, E. J., and Wolfram, J. H. (1995), Engineering scale-up of in situ bioremediation processes: a review, *Journal of Contaminant Hydrology*, 19, 171-203

Tarits, C., Aquilina, L., Ayraud, V., Pauwels, H., Davy, P., Touchard, F., and Bour, O. (2006), Oxido-reduction sequence related to flux variations of groundwater from a fractured basement aquifer (Ploemeur area, France), *Applied Geochemistry*, 21, 29-47

Thullner, M., Zeyer, J., and Kinzelbach, W. (2002), Influence of Microbial Growth on Hydraulic Properties of Pore Networks, *Transport in Porous Media*, 49, 99-122

Tompkins, J., Smith, S., Cartmell, E., and Wheater, H. (2001), In-situ bioremediation is a viable option for denitrification of Chalk groundwaters, *Quarterly Journal of Engineering Geology and Hydrogeology*, 34, 111-125

van Loosdrecht, M. C. M., Heijnen, J. J., Eberl, H., Kreft, J., and Picioreanu, C. (2002), Mathematical modelling of biofilm structures, *Antonie van Leeuwenhoek*, 81, 245-256

Vo, G. D. and Heys, J. (2011), Biofilm Deformation in Response to Fluid Flow in Capillaries, *Biotechnology and Bioengineering*, 108, 1893-1899

von Gunten, U. and Zobrist, J. (1993), Biogeochemical changes in groundwater-infiltration

systems: Column studies, *Geochimica et Cosmochimica Acta*, 57, 3895-3906

Wanner, O., Cunningham, A., and Lundman, R. (1995), Modeling Biofilm Accumulation and Mass-Transport in a Porous-Medium Under High Substrate Loading, *Biotechnology and Bioengineering*, 47, 703-712

Williamson, K. and McCarty, P. L. (1976), A Model of Substrate Utilization by Bacterial Films, *Journal Water Pollution Control Federation*, 48, 9-24

Yu, L., Xuefu, Y., and Dalin, G. (1999), Biofilm formation and control in flowing system, *Huanjing Kexue*, 20, 98-99